Conformational analysis in aqueous solution and estimation of the persistence length of exopolysaccharides produced by *Lactobacillus helveticus* Lh59 and *Streptococcus macedonicus* Sc136[1]

J. Albert van Kuik, Sébastien J.F. Vincent, Bas R. Leeflang, Loes M.J. Kroon-Batenburg, and Johannis P. Kamerling

Abstract: The conformations of two exopolysaccharides, one produced by *Lactobacillus helveticus* Lh59 and one by *Streptococcus macedonicus* Sc136, were investigated by molecular modelling to get insight into their physical properties. In particular, the influence of side chains and glycosidic linkage types on the overall shapes and persistence lengths of the polysaccharides were studied. It appeared that the side chains had only minor effects on the persistence lengths of the polysaccharides, with the exception of the monosaccharide residue directly attached to the backbone. The extensiveness of the backbone is enhanced by β-D-Hex*p*-(1→4) structural elements, whereas α-D-Hex*p*-(1→3) and α-D-Hex*p*-(1→4) elements create structural variability by introducing bends. The occurrence of either (1→5)- or (1→6)-linked monosaccharides, resulting in one extra bond between monosaccharide units, causes the overall flexibility of the polysaccharide chain to be enhanced and extensiveness to be reduced. The presence of such flexible linkages in the backbone leads to a shorter persistence length than when present in the side chain: a value of only 4.5 nm was found for the *L. helveticus* Lh59 EPS with a (1→5) linkage in the backbone, and a value of 8.5 nm for the *S. macedonicus* Sc136 EPS with two (1→6) linkages in the side chain.

Key words: conformational analysis, exopolysaccharide, *Lactobacillus helveticus*, molecular modelling, persistence length, *Streptococcus macedonicus*.

Résumé : Faisant appel à la modélisation moléculaire, on a étudié les conformations de deux exopolysaccharides, l'un produit par *Lactobacillus helveticus* Lh59 et l'autre par le *Streptococcus macedonicus* Sc136, dans le but de mieux comprendre leurs propriétés physiques. On a étudié particulièrement l'influence des chaînes latérales et les types de liaisons glycosidiques sur les formes globales et sur la longuer de persistance des polysaccharides. Il semble que les chaînes latérales n'ont que des effets mineurs sur la longuer de persistance des chaînes des polysaccharides, à l'exception du résidu monosaccharide attaché directement au squelette. L'étendue du squelette est augmentée par les éléments structuraux β-D-Hex*p*-(1→4) alors que les éléments α-D-Hex*p*(1→3) et α-D-Hex*p*(1→4) créent de la variabilité structurale en introduisant des courbures. La présence de monosaccharides liés soit en (1→5)- ou (1→6)-, qui conduit à la présence d'une liaison supplémentaire entre les unités de monosaccharides, provoque une augmentation de la flexibilité globale de la chaîne polysaccharide et à une diminution de l'étendue du squelette. La présence de telles liaisons flexibles dans le squelette conduit à une longuer de persistance moins longue que celle observée lorsqu'on les retrouve dans les chaînes latérales. La valeur de l'« EPS » pour le *L. helveticus* Lh59 comportant une liaison (1→5) dans le squelette n'est que de 4,5 nm alors que pour le *S. macedonicus* Sc136 comportant deux liaisons (1→6) dans la chaîne latérale, cette valeur est de 8,5 nm.

Mots clés : analyse conformationnelle, exopolysaccharide, *Lactobacillus helveticus*, modélisation moléculaire, longueur de persistance, *Streptococcus macedonicus*.

[Traduit par la Rédaction]

Received 19 August 2005. Published on the NRC Research Press Web site at http://canjchem.nrc.ca on 17 May 2006.

J.A. van Kuik,[2] B.R. Leeflang,[3] and J.P. Kamerling. Bijvoet Center, Department of Bio-Organic Chemistry, Utrecht University, Padualaan 8, NL-3584 CH Utrecht, The Netherlands.
S.J.F. Vincent. Nestlé Research Center, PO Box 44, Vers-chez-les-Blanc, CH-1000 Lausanne 26, Switzerland.
L.M.J. Kroon-Batenburg. Bijvoet Center, Department of Crystal and Structural Chemistry, Utrecht University, Padualaan 8, NL-3584 CH Utrecht, The Netherlands.

[1]This article is part of a Special Issue dedicated to Professor Walter A. Szarek.
[2]Deceased.
[3]Corresponding author (e-mail: b.r.leeflang@chem.uu.nl).

 doi:10.1139/V06-055

Introduction

In recent years, the interest in exopolysaccharides (EPSs) from lactic acid bacteria (LAB) has increased remarkably in the food industry, mainly because of the thickening capacities of EPSs in dairy products and the GRAS (Generally Recognized As Safe) status of the associated microorganisms (1–3). In the context of getting insight into the physical and (or) rheological properties of EPSs, conformational analysis of these biopolymers in aqueous solution is of the utmost importance. To explore this area, in an earlier investigation we have presented a method for constructing conformational models in water of heteropolysaccharides built up from repeating units, and applied this methodology to the exopolysaccharide produced by *Lactobacillus helveticus* 766 (4). Polysaccharide models were formed from oligosaccharide fragment models that were obtained from molecular dynamics (MD) simulations. The fragments were incorporated in the backbone in a ratio dictated by the population distribution of the glycosidic linkages. These were determined by the method of adaptive umbrella sampling (AUS) of the potential of mean force (PMF) (5).

When cultured in skimmed milk, *L. helveticus* Lh59, one of the attractive alternatives to replace currently used thickeners, produces a high-molecular-mass EPS ($\geq 2 \times 10^6$ Da) with a branched hexasaccharide repeating unit (Scheme 1A) (6). *Streptococcus macedonicus* Sc136, being part of the starter flora present in Greek sheep and used in goat cheese production, produces an EPS with a different branched hexasaccharide repeating unit (Scheme 1B) (7), having a large molecular-mass distribution ranging from 1×10^5 to $\geq 2 \times 10^6$ Da and highly texturizing properties. The viscosity of the growth medium was shown to be significantly reduced by alteration of the EPS side chain (7).

In the present study, the conformational properties of the EPSs of the *L. helveticus* Lh59 and *S. macedonicus* Sc136 strains were investigated. Because the presence and structure of a side chain within the repeating unit of a polysaccharide is a key element for its texturizing properties, specific attention was paid to the relation between the polysaccharide conformation in solution and the side-chain structure as well as to the persistence length of the EPSs.

Scheme 1.

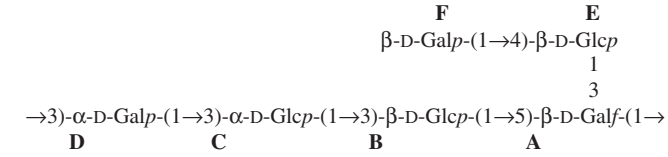

(A) *Lactobacillus helveticus* Lh59 EPS

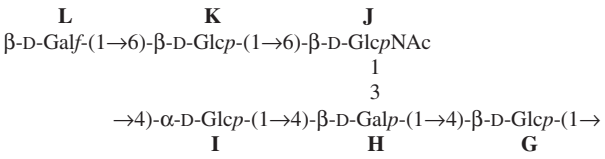

(B) *Streptococcus macedonicus* Sc136 EPS

Experimental

Nomenclature

For the three staggered conformations of the C5—C6 bonds in hexopyranoses and the C4—C5 bonds in hexofuranoses, the notation *tg*, *gt*, and *gg* was used. In this nomenclature, *g* and *t* are abbreviations of gauche (±60°) and trans (180°), respectively, indicating qualitatively the value of a dihedral angle. The angle of the O_n-C_n-C_{n-1}-O_{n-1} moiety is indicated by the first character and the angle of the O_n-C_n-C_{n-1}-C_{n-2} moiety by the second.

Isoenergy (φ, ψ) maps

Minimum energy calculations were performed using the TINKER modelling package (8). TINKER has the ability to use various common force fields such as AMBER or CHARMm. In this study we provided TINKER with the force field parameters of CHEAT (9, 10), a CHARMm-based force field where special atom types and related parameters are introduced for hydroxyl groups. In CHEAT, hydroxyl groups are represented by extended atoms to prevent the formation of intramolecular hydrogen bonds, and whereby energies are independent of the hydroxyl group orientation. Isoenergy contour maps were generated by incrementing the interglycosidic torsion angles of disaccharides in steps of 10°, producing a 36 × 36 grid. For the (1→5) and (1→6) linkage, a three-dimensional energy map was generated at a 20 × 20 × 20 resolution. Three dihedral angles per sugar ring and both interglycosidic angles were kept fixed by setting constraints during a first minimization at each grid point. For a second minimization, all constraints inside the ring were removed and the molecule was minimized again. Contour levels were plotted in steps of 1 kcal/mol (1 cal = 4.184 J), starting at the global minimum.

Molecular dynamics calculations

Molecular dynamics simulations were performed using the GROMOS-87 program package (11) and the improved force field for carbohydrates (12), on Linux computers. Each molecule was surrounded by SPC/E water molecules (13) and placed in a truncated octahedral periodic box. All bond lengths were kept fixed using the SHAKE procedure (14). Nonbonded interactions were calculated using a cutoff radius of 0.8 nm, and a time step of 2 fs. Simulations were performed with loose coupling to a pressure bath at 1 atm (1 atm = 101.325 kPa) and a temperature bath at 300 K (15) with time constants of 0.5 and 0.1 ps, respectively. A hydrogen bond is considered to be present if O-H···O < 2.5 Å, and if O-H···O angle >120°. Interglycosidic torsion angles are defined as φ (O_{ring}-$C_{1'}$-O_n-C_n), ψ ($C_{1'}$-O_n-C_n-C_{n-1}), and ω (O_n-C_n-C_{n-1}-C_{n-2}) according to IUPAC convention (16).

PMF calculations

To calculate the free energy differences of the disaccharide conformers in relation to one dihedral angle of the glycosidic linkage, PMF calculations were performed with the AUS method (5) and the GROMOS force field. All simulations were divided into jobs of 10 ps. Dihedral angle values were partitioned into 72 classes, each having a width of 5°. The derivatives of the PMF were fitted to a 12 term Fourier series. The first 0.2 ps of each job were discarded. Each system was simulated between 5 and 10 ns for

disaccharides, and up to 35 ns for the tetrasaccharide, and the final PMF was used to obtain the rotamer population distribution of the sampled dihedral angle.

Persistence length calculations

The persistence lengths of the polysaccharides were calculated similarly as has been done for cellulose (17). For cellulose, disaccharide conformational data have been used that had been selected from appropriate conformational regions of the MD simulations. For the exopolysaccharides, extended repeating units were used instead of disaccharides. For each persistence length calculation, extended repeating unit frames were selected at regular intervals from suitable MD runs, and used to randomly create 1000 polymer chains consisting of 100 repeating units each. For these compact molecules, steric hindrance can not be neglected, as could be done for cellulose. Interaction among nonbonded segments is taken into account by putting together polysaccharide models that still contain all atoms, instead of using a simplified model with vectors derived from the disaccharide building blocks. During the construction of the polysaccharide a new unit is added only after it has been checked for occupied space violations with the already existing part of the polysaccharide. The persistence length was determined by fitting the angular correlation function

$$C(j) = < \cos \vartheta_{i,i+j} >_i = \frac{< \vec{r}_i \cdot \vec{r}_{i+j} >_i}{|\vec{r}_i| \cdot |\vec{r}_{i+j}|}$$

Results and discussion

General

The *L. helveticus* Lh59 EPS is composed of a hexasaccharide repeating unit built up from a four-residue backbone, including a galactofuranose branching point, and a lactosyl side chain (Scheme 1A) (6). For this EPS the influence of the (**F**→**E**→) lactosyl side chain on the polysaccharide conformation has been evaluated through constructing polysaccharide models from MD simulations. The *S. macedonicus* Sc136 EPS is composed of a hexasaccharide repeating unit built up from three backbone residues and a trimeric side chain (Scheme 1B) (7). For this EPS separate MD simulations have been performed for repeating units with different numbers of side-chain residues attached. In fact, the influence of the (**L**→**K**→**J**→) side chain was evaluated through a conformational analysis performed on polysaccharide models consisting of (*i*) only the backbone (**I**→**H**→**G**), (*ii*) the backbone with a side chain composed of one residue attached to the branching **H** unit (**I**→[**J**→]**H**→**G**), (*iii*) the backbone with a side chain composed of two residues attached to the branching **H** unit (**I**→[**K**→**J**→]**H**→**G**), or (*iv*) the backbone with the complete side chain of three residues attached to the branching **H** unit (**I**→[**L**→**K**→**J**→]**H**→**G**). For both EPSs, specific attention has been paid to linkages with three bonds, the (1→6) linkages for hexopyranoses and the (1→5) linkages for hexofuranoses, since these linkages, when present in the backbone, induce flexibility in the polysaccharide.

Minimum energy calculations

To explore the conformational space of both EPSs, first the global and local energy minima of the glycosidic dihedral angles of the constituting disaccharide fragments in vacuo were investigated. Relaxed energy contour maps for the φ and ψ glycosidic dihedral angles were created by means of the CHEAT force field at 10° resolution. For each map generated for the (1→3) and (1→4) linkages, the energy minima differed only in ψ and have φ essentially at one position, either 60° or –60° (Fig. 1, Lh59 EPS and Fig. 2, Sc136 EPS). The (1→5) linkages for internal furanoses and the (1→6) linkages for internal pyranoses involve one extra dihedral angle (ω) and therefore three-dimensional (3D) maps were created at 18° resolution. It appeared from the 3D maps that the low energy conformations have φ essentially at –60°, with ψ either near –60° or 120° for (1→5) linkages, or near 180°, 60°, or –60° for (1→6) linkages. The angles ω were found to be near 180°, 60°, or –60°. Hence, for all (1→5) and (1→6) linkages, three (φ, ψ) maps were generated at 10° resolution, with ω at 180°, 60°, and –60°, respectively, reflecting the gauche–trans (*gt*), gauche–gauche (*gg*), and trans–gauche (*tg*) orientations of the ω angle. Moreover, one (ψ, ω) map with φ set at –60° was calculated. The results are depicted in Fig. 1 (Lh59 EPS) and Fig. 2 (Sc136 EPS). For all minimum energy positions in the maps, conformations were minimized without constraints. For each map, the obtained glycosidic dihedral angles and the relative energies of the minima are listed in Table 1.

Adaptive umbrella sampling of the PMF

The low-energy conformations in vacuo were obtained from the calculation of energy minima. Then, the population distributions of these energy minima in aqueous solution were obtained from the PMF calculated for each low energy conformer (5). Hydrogen bonds are known to play a key role in carbohydrates (18). By explicitly including water, the influence of hydrogen bonds is modelled properly. For each set of (1→3) and (1→4) linkages, only the ψ angle spanned multiple conformational regions, while the φ angle was found to be essentially constant. Therefore, the PMF was only calculated for the ψ angles. For all AUS simulations, disaccharides were used with simulation times from 5 to 10 ns.

Lactobacillus helveticus Lh59 EPS

From the PMF calculations, the population distribution can be calculated. It turned out that the (1→3) and (1→4) linkages each adopt one single dominant conformation (Table 2). From the energy maps of the (1→5) linkage, it emerged that low energy conformations have a φ angle at –60°, and a ψ angle of 140° and sometimes –60°, whereas ω takes values of 180°, –60°, or 60°. To get the population distribution for ω, an AUS run was performed for ω with φ and ψ initially set to –60° and 140°, respectively. The calculations were performed on the tetrasaccharide fragment **B**→[**E**→]**A**→**D** to incorporate the influence of long range interactions as much as possible. The result is a population distribution for the ω angle of 180°/–60°/60° = 31/67/2 (Fig. 3A). The φ and ψ dihedral angles remained close to –70° and 140°, respectively, during a 17 ns calculation. Subsequently, a 35 ns AUS run for the ψ dihedral angle was performed, again with φ initially set at –60°. This demonstrated

Fig. 1. Energy contour plots of glycosidic dihedral angles for *L. helveticus* Lh59 EPS disaccharide fragments. For the coding system, see Scheme 1A. Contours are plotted at regular intervals of 1 kcal/mol (1 cal = 4.184 J) with respect to the global energy minimum. (*a*) Global minima; (*b*)–(*f*) Local minima.

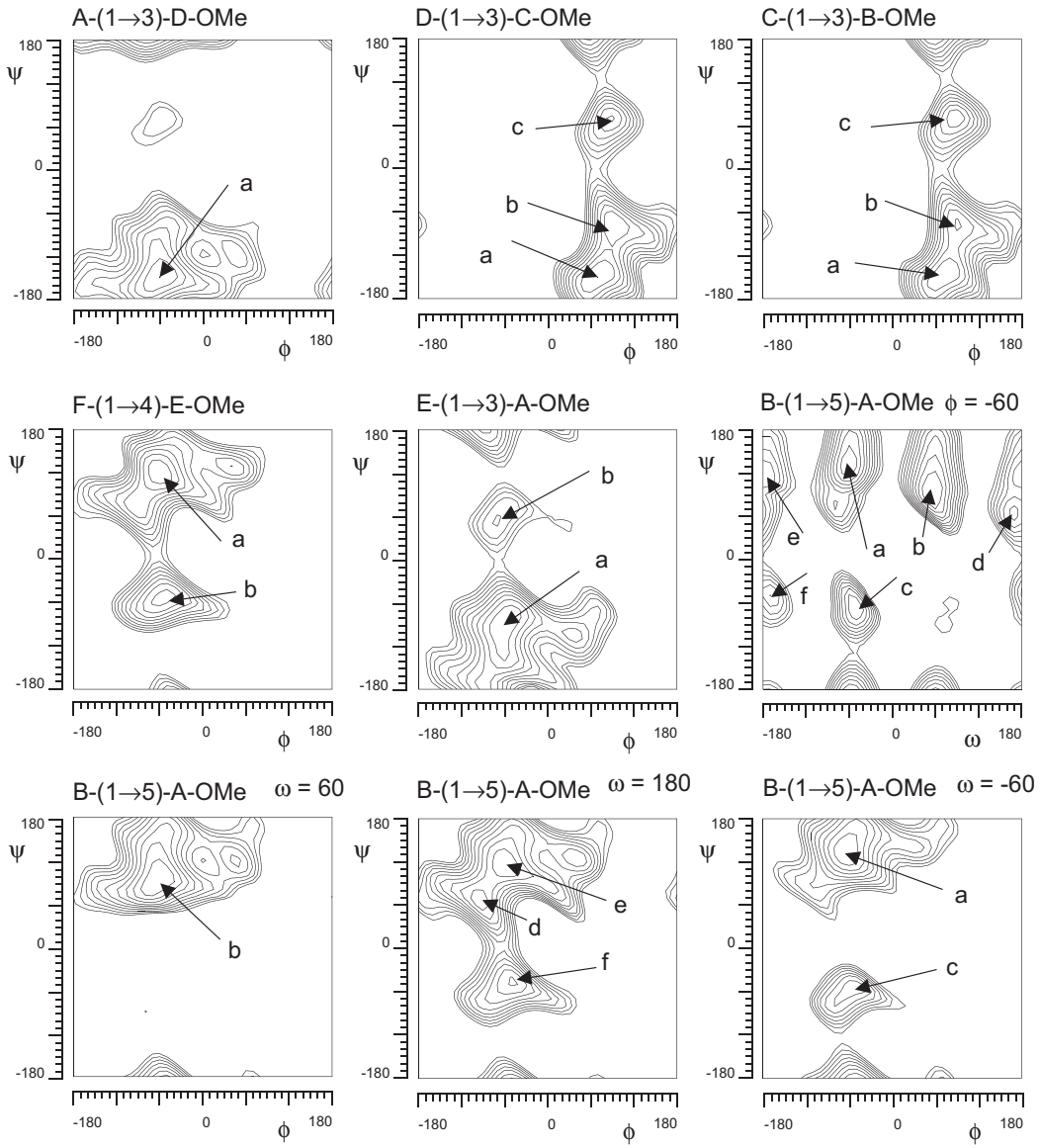

that the ψ dihedral angle has a marked preference for values around 140° (Fig. 3B). During this run, ω visited all low-energy positions that were discovered in the energy contour maps (Fig. 4B). This was in accordance with the results of the AUS run for ω, and indicates that ψ has been adequately sampled. Note that during the AUS run of dihedral ω, the ψ dihedral angle varied between 180° and 60°, and did not sample all low-energy positions that were discovered in the energy contour maps (Fig. 4A). However, this is in agreement with the population distribution of the ψ dihedral angle.

Streptococcus macedonicus Sc136 EPS

The population distributions of the (1→4) and (1→3) linkages (**G→I**, **I→H**, **H→G**, and **J→H**) showed essentially one conformational region (Table 2). From the energy maps of the (1→6) linkages, it emerged that low-energy conformations have a φ angle at –85°, a ψ angle predominantly at 180°, and ω with values of 180°, –60°, or 60°. The population distribution for ω was again obtained from AUS runs performed for the ω angle with φ and ψ initially set to –85° and 180°, respectively. The (1→6) linkages (**K→J** and **L→K**) both displayed two main conformational regions for ω of 180° and 60° (Table 2, Figs. 3C and 3D). Similarly to the (1→5) linkage in the EPS of *L. helveticus* Lh59, the ψ dihedral angle has a preference for values around 180°. Figures 4C and 4D show that ψ visited all low-energy positions during the sampling of the ω dihedral angles. The population distribution of both ω dihedral angles (Table 2) reveals that the flexibility of this polysaccharide is located mainly in the side chains.

Note that the low-energy positions and the relative energies obtained from the energy maps might deviate slightly from those resulting from the AUS method. For **B→A** (Lh59 EPS) and **L→K** (Sc136 EPS), this resulted even in different global minima.

Fig. 2. Energy contour plots of glycosidic dihedral angles for *S. macedonicus* Sc136 EPS disaccharide fragments. For the coding system, see Scheme 1B. Contours are plotted at regular intervals of 1 kcal/mol (1 cal = 4.184 J) with respect to the global energy minimum. (*a*) Global minima; (*b*)–(*g*) Local minima.

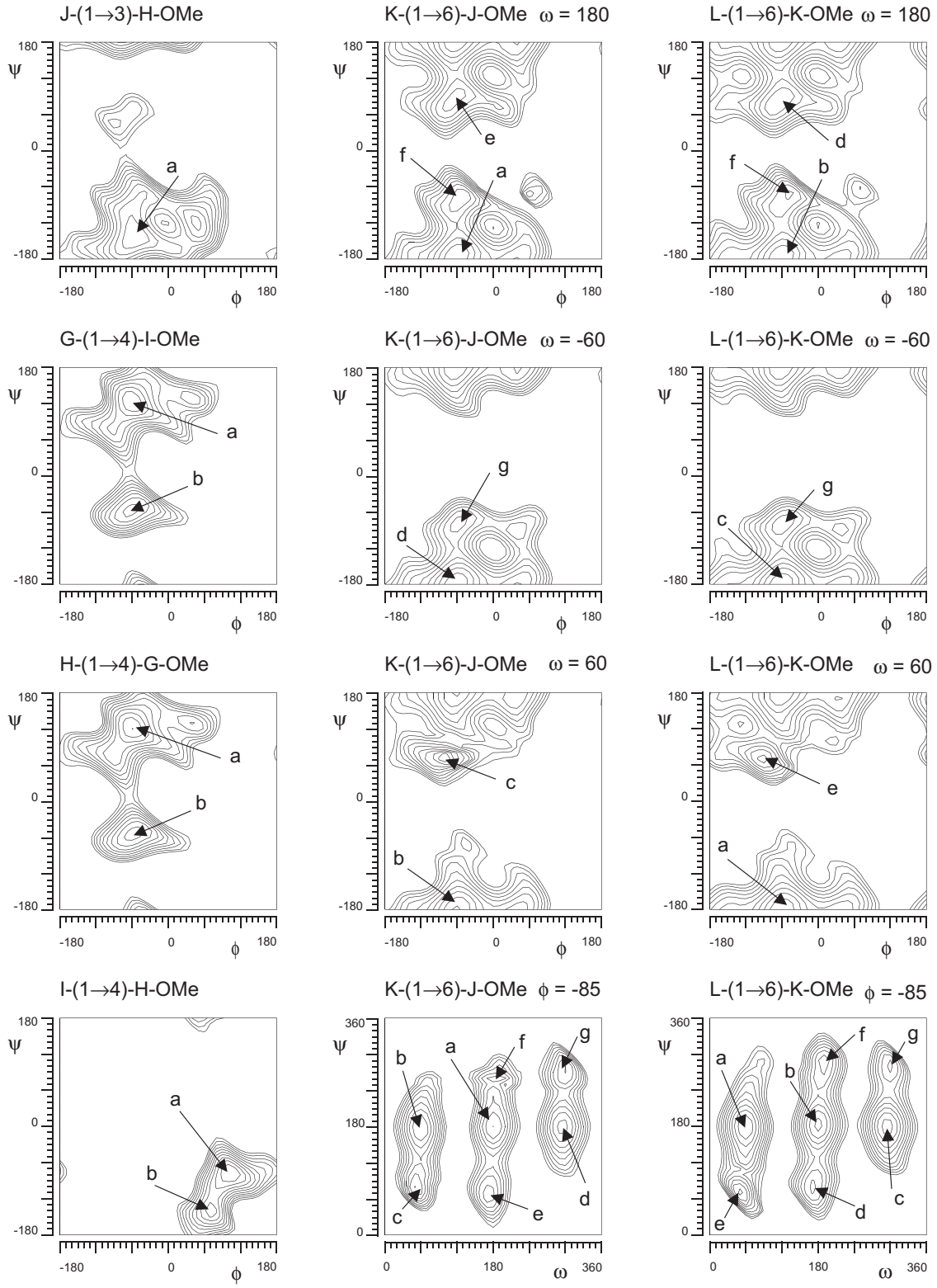

Molecular dynamics calculations

MD simulations were performed on polysaccharide fragments. The results of the AUS simulations were used to identify the most probable conformations for each fragment, which would then be used to start the MD simulations. The ω dihedral angle of the (1→5) and (1→6) linkages spanned

Table 1. Minimal energy conformations of the six constituting disaccharide fragments of *L. helveticus* Lh59 EPS and of *S. macedonicus* Sc136 EPS.

Disaccharide fragment	Minima	Dihedral angles φ	ψ	ω	ΔE^a
***L. helveticus* Lh59 EPS**					
D-(1→3)-**C**	a	59.5	–165.7		0.0
	b	87.2	–70.1		1.4
	c	84.3	68.2		3.1
C-(1→3)-**B**	a	59.8	–165.8		0.0
	b	85.5	–69.4		0.8
	c	84.3	68.8		2.3
B-(1→5)-**A**	a	–50.0	170.6	–56.8	0.0
	b	–63.6	79.1	56.4	0.6
	c	–59.4	–63.0	–53.2	1.0
	d	–83.3	60.7	173.7	3.2
	e	–53.3	103.2	179.6	5.3
	f	–52.6	–54.6	–169.2	5.8
A-(1→3)-**D**	a	–62.7	–164.8		0.0
E-(1→3)-**A**	a	–52.3	–74.2		0.0
	b	–63.6	53.2		7.4
F-(1→4)-**E**	a	–54.0	107.1		0.0
	b	–56.3	–56.0		0.2
***S. macedonicus* Sc136 EPS**					
L-(1→6)-**K**	a	–61.0	179.2	59.1	0.0
	b	–62.2	179.5	–65.5	0.3
	c	–61.8	–176.7	–179.7	1.1
	d	–72.6	73.2	169.8	1.5
	e	–86.4	73.0	52.0	2.1
	f	–47.7	–69.8	–167.0	2.7
	g	–58.0	–78.4	–60.6	3.4
K-(1→6)-**J**	a	–61.6	–175.9	–179.5	0.0
	b	–88.7	73.8	52.7	0.1
	c	–62.9	179.4	–65.8	0.5
	d	–61.1	179.8	59.0	0.7
	e	–73.2	76.5	171.8	2.1
	f	–52.0	–77.2	–168.9	2.3
	g	–56.0	–77.1	–61.0	4.1
J-(1→3)-**H**	a	–54.2	–142.0		0.0
H-(1→4)-**G**	a	–60.6	121.4		0.0
	b	–54.8	–52.3		1.6
G-(1→4)-**I**	a	–60.4	122.3		0.0
	b	–63.8	–56.5		1.6
I-(1→4)-**H**	a	102.5	–76.9		0.0
	b	71.6	–140.3		1.5

[a]Relative energy (kcal/mol).

multiple low-energy regions, making an adequate sampling during the MD calculations unlikely. Therefore, three separate simulations were started for these linkages with the most stable conformations taking ω initially set to 180°, –60°, and 60°.

Lactobacillus helveticus Lh59 EPS

All glycosidic φ and ψ dihedral angles were set at their global energy minima. The polysaccharide fragment was composed of a repeating unit (six monosaccharides) and three supplementary backbone monosaccharides (**D′→C′→B′**). These extra monosaccharides were connected to galactofuranose residue **A**, thus resulting in fragment **D→C→B→[F→E→]A→D′→C′→B′**. This was done to ensure that the branching residue **A**, likely to be a very flexible position in the backbone, might allow the sampling of conformations with long-range interactions between the side chain and the backbone of the polysaccharide. Three starting conformations were established with varying **B**-(1→5)-**A** ω angles of 180°, –60°, and 60°, respectively. For each of the starting conformations of this fragment, a 5 ns MD simulation was performed (data not shown). The MD trajectories were inspected to determine the transitions of the various dihedral angles, the formation of hydrogen bonds, and the general shape of the molecule. Trajectory-averaged dihedral angles of the MD simulations are given in Table 3. During the 5 ns

Table 2. Minimum energy values and probability distributions of the ψ and ω dihedral angles of the six constituting disaccharide fragments of *L. helveticus* Lh59 EPS and of *S. macedonicus* Sc136 EPS, as calculated by the AUS runs.

Dihedral angle		Minimum energy value (°) and population distribution (%)											
Lh59		**D**-(1→3)-**C**		**C**-(1→3)-**B**		**B**-(1→5)-**A**		**A**-(1→3)-**D**		**E**-(1→3)-**A**		**F**-(1→4)-**E**	
ψ													
		–115	(>99)	–125	(>98)	150	(>99)	–120	(>99)	–90	(>99)	110	(>99)
ω													
	(*gt*)					–170	(31)						
	(*tg*)					–75	(67)						
	(*gg*)					660	(2)						
Sc136		**L**-(1→6)-**K**		**K**-(1→6)-**J**		**J**-(1→3)-**H**		**H**-(1→4)-**G**		**G**-(1→4)-**I**		**I**-(1→4)-**H**	
ψ													
						–140	(100)	120	(>97)	120	(>97)	–120	(100)
ω													
	(*gt*)	–170	(56)	–175	(76)								
	(*tg*)	–80	(2)	–85	(2)								
	(*gg*)	60	(42)	60	(22)								

Note: Probability distributions are given in parentheses in %.

Table 3. Trajectory-averaged dihedral angles of the MD simulations of *L. helveticus* Lh59 EPS.

	Repeating unit		
	D→**C**→**B**→[**F**→**E**→]**A**→**D′**→**C′**→**B′**		
Dihedral angle	ω_{BA} = 180°	ω_{BA} = –60°	ω_{BA} = 60°
D-(1→3)-**C**			
φ	89	93	93
ψ	–135	–130	–130
C-(1→3)-**B**			
φ	95	92	94
ψ	–127	–132	–131
B-(1→5)-**A**			
φ	–77	–80	–78
ψ	142	148	135
ω	–166/–84[a]	–75/–157[b]	58
F-(1→4)-**E**			
φ	–85	–85	–86
ψ	109	109	108
E-(1→3)-**A**			
φ	–77	–78	–80
ψ	–94	–101	–98/59[c]
A-(1→3)-**D′**			
φ	–83	–86	–94
ψ	–125	–125	–132
D′-(1→3)-**C′**			
φ	92	91	91
ψ	–131	–132	–130
C′-(1→3)-**B′**			
φ	99	91	95
ψ	–123	–133	–129

[a]Transition: 180° → –60° after 2.7 ns, –60° → 180° after 2.9 ns.
[b]Transition: –60° → 180° after 2.5 ns, 180° → –60° after 2.8 ns.
[c]Transition: –100° → 60° after 4.5 ns.

simulation time, transitions observed for the ω angle were in the simulations started from conformations with ω either at 180° or –60°. For a short period of 200 ps, ω changed from 180° to –60° before returning to 180° again in the first MD simulation. Similarly, in the second MD simulation, ω changed from –60° to 180° for a short period of 300 ps and then switched back to –60°. In the third MD simulation, the glycosidic ψ angle of the disaccharide **E**→**A** showed a transition from –100° to 60° after 4.5 ns. Otherwise, it was found that the other trajectory-averaged dihedral angles were essentially the same for all MD simulations. The trajectory-averaged dihedral angles of the polysaccharide fragment were found to be similar to those calculated during the AUS simulations of the disaccharides or of the tetrasaccharide **B**→[**E**→]**A**→**D**. No major long-range hydrogen bond formation was detected in any of the MD runs. The hydrogen bonds detected for more than 7% of the simulation time were usually between neighbouring monosaccharide residues. The only exception was a hydrogen bond between **E** OH-6 and **B** OH-2 for the simulation with ω = 60°, which was observed for 50% of the simulation time. This hydrogen bond might be a stabilizing factor for this conformation. Because the conformation with ω = 60° only contributes at a level of 2% to the conformation of the polysaccharide, this was not further investigated. Conformations with ω = 180° or –60° induced a curved backbone, while ω = 60° yielded an almost straight backbone (Figs. 5A–5C).

Streptococcus macedonicus Sc136 EPS

To study the influence of the side chains on the conformational behaviour of the polysaccharide, 5 ns MD simulations were performed on polysaccharide units containing zero to three side-chain residues. The simulated molecules were relatively large fragments consisting of three repeating units. A first MD simulation was performed with a polysaccharide fragment representing the bare backbone and only consists of three times the **I**→**H**→**G** backbone unit (*i*), resulting in a fragment of nine monosaccharide residues. As expected from the energy contour maps and the AUS calculations of the PMF, all linkages were found almost exclusively in one conformational region (Table 4). This clearly showed that the backbone of the Sc136 EPS is more rigid than that of the Lh59 EPS. The second MD simulation (*ii*) was made with the fragment in (*i*) extended with one

Fig. 3. Population distributions of the (1→5) glycosidic (A) ω dihedral angle and (B) ψ dihedral angle of *L. helveticus* Lh59 EPS. Population distributions of the (1→6) glycosidic ω dihedral angles of (C) K→**J** and (D) **L**→**K** of *S. macedonicus* Sc136 EPS.

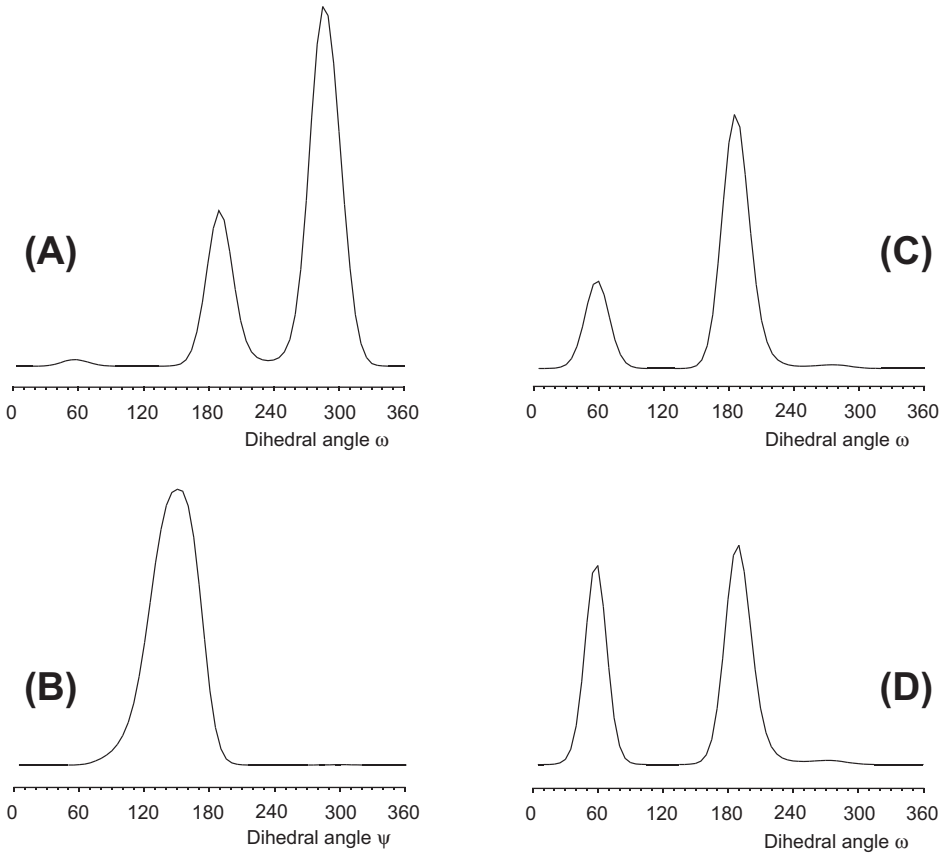

Fig. 4. Scatter plots of the (1→5) glycosidic ψ and ω dihedral angles of the AUS run of (A) the ω angle and (B) the ψ angle of *L. helveticus* Lh59 EPS. Scatter plots of the (1→6) glycosidic ω dihedral angles of the AUS runs of ω of (C) **K**→**J** and (D) **L**→**K** of *S. macedonicus* Sc136 EPS. For the coding system of the minima, see Figs. 1 and 2.

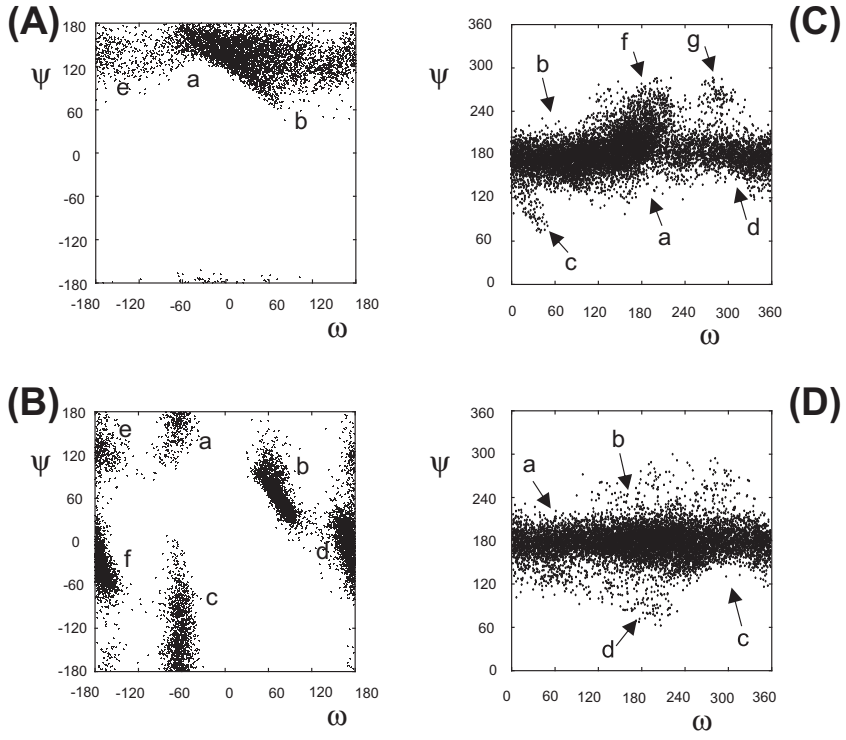

Fig. 5. The three most probable conformations of a repeating unit of *L. helveticus* Lh59 EPS, (A) $B_{180}\rightarrow$**A**, (B) $\mathbf{B}_{-60}\rightarrow$**A**, and (C) $\mathbf{B}_{60}\rightarrow$**A**. The four most probable conformations of a repeating unit of *S. macedonicus* Sc136 EPS, (D) $\mathbf{L}_{180}\rightarrow\mathbf{K}_{180}\rightarrow$**J**, (E) $\mathbf{L}_{60}\rightarrow\mathbf{K}_{180}\rightarrow$**J**, (F) $\mathbf{L}_{180}\rightarrow\mathbf{K}_{60}\rightarrow$**J**, and (G) $\mathbf{L}_{60}\rightarrow\mathbf{K}_{60}\rightarrow$**J**. A ribbon is drawn to visualize the backbone of the polysaccharides. Monosaccharide residues belonging to one repeating unit are drawn in bold.

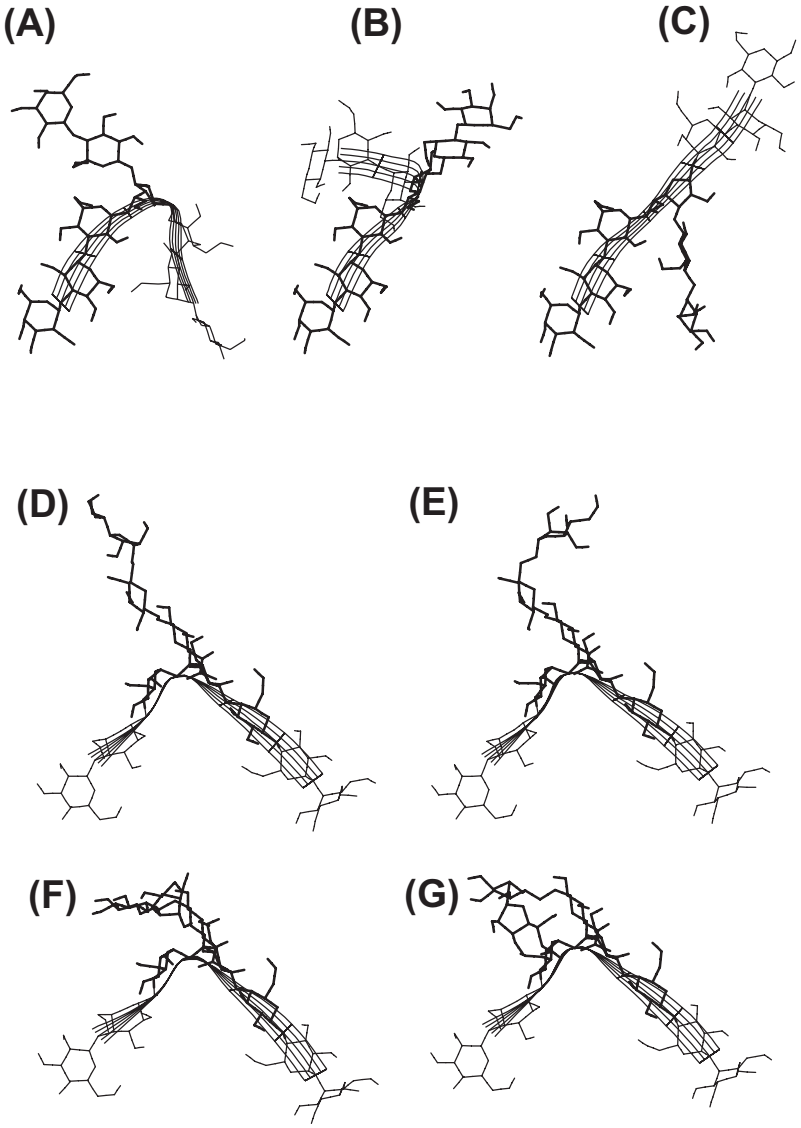

side chain monosaccharide **J** for each repeating unit, resulting in a fragment composed of three **I**→[**J**→]**H**→**G** units. Again, each linkage was confined to its most stable conformation. For the following two MD simulations, the fragment in (*ii*) was further extended with monosaccharide **K** on each repeating unit, defining a fragment consisting of three **I**→[**K**→**J**→]**H**→**G** units. The MD simulations were performed with (*iii*) $\mathbf{I}\rightarrow[\mathbf{K}_{180}\rightarrow\mathbf{J}\rightarrow]\mathbf{H}\rightarrow\mathbf{G}$ (ω_{KJ} = 180°) and (*iv*) $\mathbf{I}\rightarrow[\mathbf{K}_{60}\rightarrow\mathbf{J}\rightarrow]\mathbf{H}\rightarrow\mathbf{G}$ (ω_{KJ} = 60°). A simulation with ω_{KJ} = –60° was not considered because of the low probability (2%) of the associated conformation. The conformations of the two "external" repeating units (numbered 1 and 3) were chosen to be the same as the central unit (numbered 2). Only during the first MD simulation (*iii*) a transition did occur. The ω_{KJ} angle (middle unit) switched from 180° to –60° and back to 180° after 400 ps. In the last series of MD simulations monosaccharide **L** was added, completing the repeating unit **I**→[**L**→**K**→**J**→]**H**→**G**. Four different MD simulations were performed with (*v*) $\mathbf{I}\rightarrow[\mathbf{L}_{180}\rightarrow\mathbf{K}_{180}\rightarrow\mathbf{J}\rightarrow]\mathbf{H}\rightarrow\mathbf{G}$ (ω_{LK} = 180°, ω_{KJ} = 180°), (*vi*) $\mathbf{I}\rightarrow[\mathbf{L}_{60}\rightarrow\mathbf{K}_{180}\rightarrow\mathbf{J}\rightarrow]\mathbf{H}\rightarrow\mathbf{G}$ (ω_{LK} = 60°, ω_{KJ} = 180°), (*vii*) $\mathbf{I}\rightarrow[\mathbf{L}_{180}\rightarrow\mathbf{K}_{60}\rightarrow\mathbf{J}\rightarrow]\mathbf{H}\rightarrow\mathbf{G}$ (ω_{LK} = 180°, ω_{KJ} = 60°), and (*viii*) $\mathbf{I}\rightarrow[\mathbf{L}_{60}\rightarrow\mathbf{K}_{60}\rightarrow\mathbf{J}\rightarrow]\mathbf{H}\rightarrow\mathbf{G}$ (ω_{LK} = 60°, ω_{KJ} = 60°). The four different conformations for each repeating unit are shown in Figs. 5D–5G. In MD simulation (*v*), the ω_{KJ} angle (middle unit) went from 180° to –100° and back to 180° after 3 ns. In the same simulation, the ω_{LK} (first unit) went from 180° to 60° after 2 ns, while ω_{LK} (middle unit) went from 180° to 60° after 3 ns. During MD simulation (*vi*), all ω dihedral angles kept the initial conformation during the simulation. In MD simulation (*vii*), the ω_{KJ} angle (first unit) went from 60° to 180° after 500 ps. A simulation (*viii*) with ω_{LK} = 60° and ω_{KJ} = 60° was started three times, but within a few ps, ω_{LK} or ω_{KJ} (in the middle unit) jumped from 60° to 180°. It seems that ω = 60° for

Table 4. Trajectory-averaged dihedral angles of the 5 ns MD simulations of the central repeating unit in fragments comprising three repeating units of *S. macedonicus* Sc136 EPS.

	Repeating unit Simulation						
	I→H→G	**I→[J→]H→G**	**I→[K→J→]H→G**		**I→[L→K→J→]H→G**		
Dihedral angle	(*i*)	(*ii*)	(*iii*)	(*iv*)	(*v*)	(*vi*)	(*vii*)
I-(1→4)-**H**							
φ	106	99	100	113	94	99	118
ψ	–99	–108	–109	–96	–116	–111	–96
H-(1→4)-**G**							
φ	–78	–82	–79	–81	–84	–85	–79
ψ	109	111	112	110	110	108	113
G-(1→4)-**I**							
φ	–87	–81	–86	–91	–82	–86	–83
ψ	110	109	108	108	114	107	108
J-(1→3)-**H**							
φ		–91	–92	–91	–98	–98	–92
ψ		–127	–131	–134	–138	–138	–134
K-(1→6)-**J**							
φ			–84	–85	–84	–84	–83
ψ			–167	174	–173/–109[a]	–159	176
ω			–164[b]	59	–170	–172	60
L-(1→6)-**K**							
φ					–88	–87	–85
ψ					171	172	180
ω					–168/58[c]	58	–168

[a]Transition: 180° → –100° after 10 ps, –100° → 180° after 3 ns.
[b]Transition: 180° → –60° after 3.2 ns, –60° → 180° after 3.6 ns.
[c]Transition: 180° → 60° after 3 ns.

both (1→6) linkages does not result in a stable conformation. Therefore, this conformation is not used in the rest of the work. Figure 5 shows that the **H→G** and **G→I** segments have a linear conformation, while the **I→H** segment introduces a turn in the backbone. The **J→H** segment points away from the backbone into the solution.

Constructing polysaccharide models

The data generated by the MD simulations were used to construct a number of polysaccharide models with lengths between 10 and 500 repeating units. To this end, configurations were selected randomly from the MD runs choosing suitable conformations based on their statistical representation in the runs. The chosen repeating unit was then attached to the "growing" chain by a homemade polysaccharide-building program, which checked for space-filling constraints and prevented van der Waals clashes. Although the polysaccharide models themselves are grown in vacuo, the models do represent polysaccharides in aqueous solution because the applied building blocks are directly transferred from MD simulations in the presence of water. Since the interaction between water and the saccharides is very dynamic — no "sticky" water molecules have been observed during the MD simulations — no persistent influence is expected on the spatial arrangement of the building blocks.

Lactobacillus helveticus Lh59 EPS

Configurations were selected randomly from the MD runs of **D→C→B→[F→E→]A→D′→C′→B′** with ω = 180°/–60°/60° in a ratio of 31:67:2. Connections were made by the attachment of residue **C′** of one configuration to residue **B** of the next configuration, in addition to the removal of redundant residues (**B′**, **D**, and **C**). The newly attached fragments were checked for steric overlap with the already present part of the polysaccharide and, if needed, replaced with other fragments until no overlap occurred. Visual inspection showed a flexible structure with a secondary conformation presenting zigzags and a random coil tertiary conformation for *L. helveticus* Lh59 EPS. The galactofuranose units induced a twist in the backbone and all lactosyl side chains were extended into the solvent. A model that demonstrates the general shape of the polysaccharide is depicted in Fig. 6A.

Streptococcus macedonicus Sc136 EPS

Configurations were again selected randomly from appropriate MD runs. Connections were made by attaching residue **G** of one configuration to residue **I** of the next configuration, and removing the redundant first and last repeating units. Again, newly attached fragments were checked for steric overlap with the already present part of the polysaccharide and, if needed, replaced with other fragments until no overlap occurred. Visual inspection shows a secondary conformation that consisted of a stretched β-D-Gal*p*-(1→4)-β-D-Glc*p*-(1→4)-α-D-Glc*p* part, and then a curve where α-D-Glc*p* connects to β-D-Gal*p*. This leads to an overall "random coil" spatial conformation. The side chains were found to be very flexible, but did not seem to influence the secondary conformation. Therefore, the shape of *S. mace-*

Fig. 6. Polysaccharide models consisting of 20 repeating units. The monosaccharide residues that comprise the backbone of the polysaccharide are drawn in bold. (A) Model of *L. helveticus* Lh59 EPS. (B) Model of *S. macedonicus* Sc136 EPS.

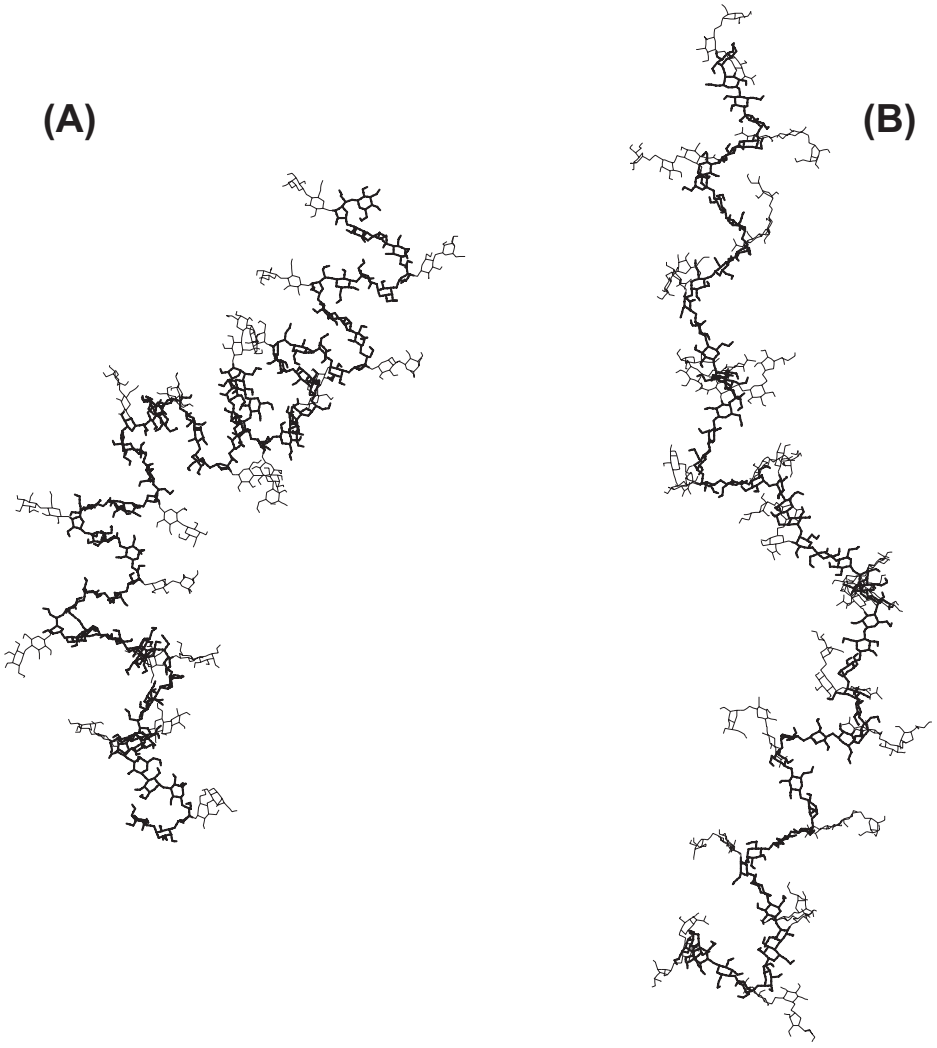

donicus EPS is mainly determined by the rigid backbone. A model that demonstrates the general shape of the polysaccharide is depicted in Fig. 6B.

Persistence length calculations

Finally, the stiffness of the polysaccharides was estimated by calculating the persistence length L_p (17), which was statistically derived from 1000 generated polysaccharide structures with a length of 100 repeating units each. The results are compiled in Table 5.

The persistence length is a measure for the "extensiveness" of a polysaccharide. The occurrence of disaccharide linkages with multiple (and populated) glycosidic conformations has enormous lowering effects on the L_p. This almost always applies to (1–6) linkages. Similar effects are observable for variations in the carbohydrate ring structure as is most prominent for furanose rings. Smaller effects are caused by the natural variation between snapshots of a "single" conformation. Here the width of the glycosidic potential energy wells plays a role. The presence of steric effects (e.g., induced by side chains) will narrow these potential energy wells resulting in an increased persistence length.

Lactobacillus helveticus Lh59 EPS

Calculation of the L_p yielded a value of 4.5 nm. The EPS turned out to be flexible and compact. By comparison, the L_p of the very stiff polysaccharide cellulose was estimated to be 14 nm (17). Steric interactions were also shown to have a considerable influence on the L_p value as demonstrated by calculations of the L_p without checking for steric overlap: a value of 2.2 nm was found, being a reduction of the L_p value by a factor of two. In addition, L_p calculations were performed on polysaccharides where the side chain had been either shortened or removed. Note that this was done with configurations from the MD simulations of the intact side chain. The side chain was only been trimmed prior to the building process. Thus, the effect on the L_p only reflects the steric hindrance during the construction of the polysaccharides. Nevertheless, as the side chains did not show many interactions with the backbone during the MD simulations, even for "long" side chains, the assumption was made that this approximation was in essence valid.

Streptococcus macedonicus Sc136 EPS

All models, except for the bare backbone (**I→H→G**),

Table 5. Persistence length (L_p) and average length of the repeating unit (l) of *L. helveticus* Lh59 EPS and *S. macedonicus* Sc139 EPS that were built from tri-, tetra-, penta-, and hexa-meric repeating units from MD simulations in water.

Repeating unit	L_p (nm)	l (nm)
Lh59		
D→C→B→[F→E→]A	4.5	1.05
D→C→B→[E→]A	4.2	1.05
D→C→B→A	3.7	1.05
D→C→B→[F→E→]A[a]	2.2	1.04
Sc136		
I→H→G	6.5	1.00
I→[J→]H→G	8.9	1.13
I→[K_{180}→J→]H→G	10.5	1.08
I→[K_{60}→J→]H→G	9.5	0.97
I→[K→J→]H→G	8.7	1.06
I→[L_{180}→K_{180}→J]H→G	10.1	1.19
I→[L_{60}→K_{180}→J→]H→G	8.1	1.12
I→[L_{180}→K_{60}→J→]H→G	9.3	1.07
I→[L→K→J→]H→G	8.5	1.14

Note: When an exclusive conformational region is used for the **K**-(1→6)-**J** and **L**-(1→6)-**K** glycosidic linkages, this is indicated by 180 or 60.

[a]No excluded volume effects were taken into account.

showed a similar L_p of ~8.7 nm. For **I→[J→]H→G**, **I→[K→J→]H→G**, and **I→[L→K→J→]H→G**, the persistence lengths were found to be 8.9, 8.7, and 8.5 nm, respectively. The bare backbone (**I→H→G**) yielded an L_p of 6.5 nm, thereby indicating a higher flexibility. From these results it can be deduced that only the first side-chain residue (**J**) influences the L_p of the polysaccharide in such a way as to strech the polysaccharide, a finding that can be explained by the position of **J** in close contact with the **I→H→G** backbone.

Conclusions

The conformational analysis method used in this paper allowed one to explicitly include the key influence of water solvation. The secondary structures of both polysaccharides studied showed a twisted backbone with side chains extending in the solvent. The main flexibility was found to be located in the intrinsically flexible (1→5) or (1→6) linkages, as well as in the furanose ring form. For *L. helveticus* Lh59 EPS, this flexibility is located in the backbone, resulting in a more compact overall shape. Analysis of the polysaccharide models showed no interactions between side chains and backbone except for the linkage point, and generally no long-range interaction among backbone units. Therefore, for the polysaccharides studied, the conclusion is that the extrapolation of small oligosaccharide fragments to polysaccharides was well-justified.

The general shape of the polysaccharides was found to be compact. This was expressed by the values obtained for the calculated persistence length. In this study, we have taken into account only the most probable conformations of the glycosidic linkages. Neglecting the less-occurring conformations may have had some influence on the calculated persistence length, since some of those minor conformations could introduce sharp bends in the backbone of the polysaccharide. Nevertheless, the dominant conformations used for the construction of the polysaccharide models and the sizes of the fragments used were large enough to include all intermonomer interactions.

The conformation of the side chains was shown to have only a small influence on the flexibility and the persistence length of the polysaccharide. Only the first residue of the side chain, linked directly to the backbone, had a clear influence. It reduced the flexibility of the backbone and made the chain stiffer. The backbone glycosidic linkages largely determined the overall shapes of the polysaccharides. The fully stretched parts were stemming from the β-D-Hex*p*-(1→4) elements, similarly as is the case for the β-D-Glc*p*-(1→4) elements in cellulose. The structural elements, α-D-Hex*p*-(1→4) and α-D-Hex*p*-(1→3), introduced bends in the backbone, thereby reducing the calculated persistence length. As the distance O4—O1 in a 4-substituted monosaccharide is longer than the distance O3—O1 in a 3-substituted monosaccharide, (1→4) linkages usually produce a longer residue length (l) than (1→3) linkages. Backbone three-bond linkages (φ, ψ, and ω) gave rise to a large variation in conformations, enhancing the flexibility and giving shorter persistence lengths.

Acknowledgments

SJFV acknowledges the constant support of Dr. J.-R. Neeser (Nestlé Switzerland).

References

1. L. De Vuyst, F. De Vin, F. Vaningelgem, and B. Degeest. Int. Dairy J. **11**, 687 (2001).
2. A.P. Laws and V.M. Marshall. Int. Dairy J. **11**, 709 (2001).
3. P. Duboc and B. Mollet. Int. Dairy J. **11**, 759 (2001).
4. E.J. Faber, J.A. van Kuik, J.P. Kamerling, and J.F.G. Vliegenthart. Biopolymers, **63**, 66 (2002).
5. R.W.W. Hooft, B.P. van Eijck, and J. Kroon. J. Chem. Phys. **97**, 6690 (1992).
6. F. Stingele, J. Lemoine, and J.-R. Neeser. Carbohydr. Res. **302**, 197 (1997).
7. S.J.F. Vincent, E.J. Faber, J.-R. Neeser, F. Stingele, and J.P. Kamerling. Glycobiology, **11**, 131 (2001).
8. J.W. Ponder. TINKER: Software tools for molecular design. Washington University School of Medicine, St. Louis, Missouri. 2000.
9. P.D.J. Grootenhuis and C.A.G. Haasnoot. Mol. Simul. **10**, 75 (1993).
10. M.L.C.E. Kouwijzer and P.D.J. Grootenhuis. J. Phys. Chem. **99**, 13426 (1995).
11. W.F. van Gunsteren and H.J.C. Berendsen. GROMOS-87: Groningen molecular simulation program package. University of Groningen, The Netherlands. 1987.
12. S.A.H. Spieser, J.A. van Kuik, L.M.J. Kroon-Batenburg, and J. Kroon. Carbohydr. Res. **322**, 264 (1999).
13. H.J.C. Berendsen, J.R. Grigera, and T.P.J. Straatsma. Phys. Chem. **91**, 6269 (1987).
14. J.-P. Ryckaert, G. Giccotti, and H.J.C. Berendsen. Comput. Phys. **23**, 327 (1977).
15. H.J.C. Berendsen, J.P.M. Postma, W.F. van Gunsteren, A. DiNola, and J.R. Haak. J. Chem. Phys. **81**, 3684 (1984).

16. IUPAC-IUB Joint Commission on Biochemical Nomenclature. Eur. J. Biochem. **131**, 5 (1983).
17. L.M.J. Kroon-Batenburg, P.H. Kruiskamp, J.F.G. Vliegenthart, and J. Kroon. J. Phys. Chem. **B101**, 8454 (1997).
18. K.N. Kirschner and R.J. Woods. Proc. Natl. Acad. Sci. U.S.A. **98**, 10541 (2001).